Title: Mechanism of connexin channel inhibition by mefloquine and 2-aminoethoxydiphenyl borate

Authors: Pia Lavriha[1,†], Yufei Han[1,†], Xinyue Ding[1], Chao Qi[1,2,3], Anand Vaithia[1], and Volodymyr M. Korkhov[1,2*]

Affiliations:

[1] Laboratory of Biomolecular Research, Paul Scherrer Institute, Villigen, Switzerland.

[2] Institute of Molecular Biology and Biophysics, ETH Zurich, Switzerland.

[3] Medical Research Council Laboratory of Molecular Biology, Cambridge, UK

[†] These authors contributed equally

*Corresponding author: volodymyr.korkhov@psi.ch

Abstract: Gap junction intercellular communication (GJIC) between two adjacent cells involves direct exchange of cytosolic ions and small molecules via connexin gap junction channels (GJCs). Connexin GJCs have emerged as drug targets, with small molecule connexin inhibitors considered a viable therapeutic strategy in several diseases. The molecular mechanisms of GJC inhibition by known small molecule connexin inhibitors remain unknown, preventing the development of more potent and connexin-specific therapeutics. Here we show that two GJC inhibitors, mefloquine (MFQ) and 2-aminoethoxydiphenyl borate (2APB) bind to Cx32 and block dye permeation across Cx32 hemichannels (HCs) and GJCs. Cryo-EM analysis shows that 2APB binds to "site A", close to the N-terminal gating helix of Cx32 GJC, restricting the entrance to the channel pore. In contrast, MFQ binds to a distinct "site M", deeply buried within the pore. MFQ binding to this site modifies the electrostatic properties of Cx32 pore. Mutagenesis of V37, a key residue located in the site M, renders Cx32 HCs and GJCs insensitive to MFQ-mediated inhibition. Moreover, our cryo-EM analysis, mutagenesis and activity assays show that MFQ targets the M site in Cx43 GJC similarly to Cx32. Taken together, our results point to a conserved inhibitor binding site in connexin channels, opening a new route for development of specific drugs targeting connexins.

One-Sentence Summary: Inhibition of Cx32 and Cx43 channels via functionally relevant drug binding sites

Introduction

Connexins are transmembrane proteins which assemble into hexameric hemichannels (HCs) at the cell surface allowing the exchange of small solutes (ions and molecules of molecular weight below ~1.5 kDa) between the cell cytoplasm and the extracellular environment [1]. Two HCs at the surface of the neighboring cells can dock in a head-to-head fashion, forming gap junction channels (GJCs) [2]. The GJCs connect the cytoplasms of neighboring cells and ensure their electrochemical and metabolic coupling in a process called gap junction intercellular communication (GJIC) [1–3]. There are 21 connexin isoforms in humans, with distinct tissue distribution, channel properties and regulatory mechanisms [2]. These channels are responsible for a variety of essential functions including cardiac contraction [4], central and peripheral nervous system signaling [5,6], tissue differentiation [7], immunity [8] and cell growth [9]. Connexin-mediated solute permeation must be tightly controlled, as highlighted by the numerous pathologies stemming from connexin mutations or dysregulation [10]. The diseases linked to connexin channels, or connexinopathies, include oculodentodigital dysplasia [11], palmoplantar keratoderma [12], keratitis-ichtyosis-deafness (KID) syndrome [13], multiple types of cancer [9,14] (reviewed in [15]).

Given the crucial role connexin channels play in health and disease they have emerged as candidate targets for drug development [16]. Inhibition of connexin GJCs and HCs, such as Cx26 and Cx43, has been suggested to be a promising strategy in treatment of KID syndrome (Cx26) [17], arrhythmias (Cx43) [18], and in acceleration of wound healing (Cx43) [19]. To this end, connexin channels have been shown to be inhibited by RNA, peptides, antibodies, and small molecules. The latter are particularly attractive as classical pharmacological agents, and a substantial amount of work has been done to characterize small molecule drug-mediated connexin inhibition. For example, glycerrhetinic acid and its derivatives [20], long-chain alcohols [21,22], fatty acids [23], quinine and its analogs [24–26] have been identified as inhibitors of connexin HC and GJC function. The substantial problem with all of these inhibitors lies in their limited connexin isoform selectivity [27]. Furthermore, despite the availability of high-resolution structures of several connexin channels, the structural basis of connexin channel inhibition by small molecule inhibitors (as well as any other types of inhibitors) is lacking.

Two widely used small molecule connexin inhibitors are mefloquine (MFQ) and 2-aminoethoxydiphenyl borate (2APB) (**Fig. 1a**). MFQ, a compound on the World Health Organization (WHO) Model List of Essential Medicines, is an antimalarial compound that targets the *Plasmodium falciparum* ACBP [28]. Administration of MFQ is associated with neurological [29], neuropsychiatric [30], hepatic [31], and gastrointestinal side effects [28]. MFQ has been shown to be a specific inhibitor of Cx36 and Cx50, capable of blocking Cx26, Cx32, and Cx43 at higher concentrations [26]. In combination with donepezil or amitriptyline, MFQ is currently tested in pre-clinical models for treatment of connexin-related disorders linked to Alzheimer disease (Cx36) and neuropathic pain (Cx43), respectively [16,32]. The second connexin inhibitor, 2APB, has been shown to have cardioprotective, anti-inflammatory, and anti-oxidative properties [33,34], inhibiting a range of connexin channels (Cx26, Cx36, Cx32, Cx40 and Cx45 HCs and GJCs) among other targets [35,36]. Understanding the molecular basis of connexin inhibition by MFQ and 2APB would enable structure-based discovery and development of drugs that target these channels in a variety of connexin-related pathologies. Moreover, development of highly specific connexin-targeting drugs with fewer side effects would be highly desirable.

To gain insights into the mechanism of connexin channel inhibition by small molecules, we analysed the structures of Cx32 in the presence of MFQ and 2APB and performed functional analysis of the drug effects *in vitro* and *in cellulo*. Our results reveal two previously undescribed modes of Cx32 channel inhibition by these two drugs. The primary mechanism of MFQ-mediated inhibition involves a conserved drug binding site deep within the pore of Cx32, Cx43 (this study) and Cx36 (a companion study) [37]. Furthermore, 2APB additionally engages a distinct binding site close to the pore entrance of Cx32.

Results

Cx32 inhibition by MFQ and 2APB. The effects of MFQ and 2APB on Cx32 have been previously investigated. MFQ was shown to inhibit Cx32 GJC-mediated coupling in RIN cells [38], and reduce the

junctional currents in N2A cells [26]. 2APB was shown to inhibit purified Cx32 HCs and Cx32 GJC-mediated dye-coupling in HeLa cells [35], but did not affect junctional conductance in Cx32-coupled N2A cells [36]. To assess the effect of these drugs on Cx32 HCs and GJCs we performed HC dye uptake assays and gap-fluorescence recovery after photobleaching (gap-FRAP) experiments (**Fig. 1b-c, e-f**). We used HEK293F cells which express Cx32 at the plasma membrane [39] and form functional gap junctions (Extended Data Fig. 1). Both drugs inhibited the Cx32 HC activity (**Fig. 1b,e**) and the GJC-mediated dye transfer (**Fig. 1c,f**, Extended Data Fig. 2a-b). Both drugs were also able to bind to the purified Cx32 (Extended Data Fig. 3), as shown by the intrinsic tryptophan fluorescence quenching-based binding assays (**Fig. 1d,g**, Extended Data Fig. 4). Analysis of the MFQ binding data using non-linear regression with a one-site specific binding model resulted in an estimate of a binding constant of 43.1 μM (**Fig. 1d**). For 2APB, fitting the tryptophan emission shift data to a two-site specific binding model resulted in apparent high and low affinity binding constants of 1.05 μM and 75.1 μM, with both sites occupied approximately equally (**Fig. 1g**).

Structural analysis of Cx32 GJCs in complex with MFQ or 2APB. To determine the location of the drug binding sites in Cx32 and to assess the effects of the drugs on the channel structure, we prepared single particle cryo-EM samples of purified Cx32 (Extended Data Fig. 3a) in the presence of MFQ and 2APB. Using cryo-EM analysis and image processing we obtained 3D reconstructions of the Cx32 GJCs in D6 symmetry bound to MFQ at 2.91 Å resolution (Extended Data Figs. 5, 7a) and to 2APB at 2.86 Å resolution (Extended Data Figs. 6, 7c; Extended Data Fig. 10a,c, Extended Data Table 1). The quality of the density maps was sufficient to resolve all of the features of the Cx32 GJC structure [39], namely the transmembrane helices (TM1-4), extracellular loops 1 and 2 (ECL1-2) and lipid or detergent-like densities on the protein-lipid interface (Extended Data Fig. 8a, 9a). In addition to these expected structural elements each of the maps revealed features specific to the added drugs, as detailed below.

Focusing on the Cx32 HC particles (Extended Data Figs. 5b, 6b) allowed us to obtain the cryo-EM reconstructions of Cx32 HCs in the presence of MFQ and 2APB at 3.46 Å and 3.14 Å resolution, respectively, in C6 symmetry (Extended Data Fig. 5c, 6c, 7b,d, 8b, 9b). Since the analysis of Cx32 HC in complex with 2APB and MFQ revealed differences to Cx32-apo HC [39] that were difficult to unambiguously interpret, we have focused our analysis on the GJC structures (Extended Data Fig. 11).

Additional densities corresponding to MFQ and 2APB in Cx32 reconstructions. Addition of MFQ to Cx32 GJC did not alter the overall conformation of the channel, with an RMSD of 0.447 Å between the Cx32-apo [39] and the Cx32-MFQ (**Fig. 2**). The N-terminal helix (NTH) remained unresolved, similar to the Cx32-apo GJC structure (**Fig. 1h, Fig. 2b**). However, an additional density element was clearly present in the pore region corresponding to the previously described lipid-1 site. We interpret this density as the site of MFQ binding, and thus this region of Cx32 is referred to as "site M".

Although overall the difference between Cx32-apo and Cx32-2APB was very small in the transmembrane and extracellular domains (0.344 Å), addition of 2APB caused a clear conformational change in the Cx32 GJC (**Fig. 1i, Fig. 2c**). The NTH, flexible in the apo- and MFQ-bound forms of the channel, changed to a conformation closely resembling the NTH conformation in the Cx32-apo HC structure [39]. An additional density between the NTH regions of the neighboring Cx32 monomers likely corresponds to 2APB. We refer to this region of the protein as "site A". Moreover, a poorly resolved additional density is present in the site M (**Fig. 2d,** Extended Data Fig. 10), potentially indicative of weak binding of 2APB to this drug binding pocket, in addition to site A.

To investigate the MFQ and 2APB binding sites, we have compared the site A and site M densities in the reconstructions of Cx32-apo, Cx32-MFQ and Cx32-2APB GJCs (**Fig. 2d,** Extended Data Fig. 10). Upon addition of MFQ, the only change in Cx32 GJC density occurs at site M. This density is large enough to accommodate the quinoline part of the molecule. However, there is no clearly defined density which fits the piperazine moiety of either (+)-(11*R*, 12*S*) or (-)-(11*S*, 12*R*) enantiomer of MFQ, both of which were present in the sample (Extended Data Fig. 10a). As accurate positioning of MFQ is not possible, we modelled the MFQ based on its conformation in a complex with Cx36 GJC, for which a high-resolution 3D reconstruction is available. In the case of 2APB, the site M density only allows

134 approximate placement of the drug, whereas site A is sufficiently resolved for more reliable modeling
135 of the molecule (Extended Data Fig. 10b).

136 To assess the variability in drug binding among individual Cx32 subunits we performed protomer-
137 focused classification (PFC) [40] of Cx32 GJC in complex with MFQ and 2APB (Extended Data Fig. 12).
138 The classification did not result in 3D classes with improved MFQ density and did not allow the
139 separation between the two enantiomers. However, classes 1 and 5 revealed that not all subunits were
140 occupied by the drug, whereby class 1 also contained a somewhat better resolved N-terminus lining the
141 Cx32 pore. Similar to MFQ, PFC did not yield a class with either of the 2APB binding sites better
142 resolved. The low resolution of the 3D reconstructions prevented us from quantitatively assessing the
143 differences in site A and site M occupancies. Nevertheless, the classification confirmed that there is
144 some variability in the NTH of the subunits constituting the drug-bound GJC.

145 **Binding of 2APB to site A.** The NTH in Cx43 has been previously shown to bind lipids, presumably
146 stabilizing the NTH in the closed conformation [40,41]. The site A in Cx32-2APB is located at this region,
147 between the NTH of the neighboring subunits (**Fig. 3a,** Extended Data Fig. 13a). The phenyl rings of
148 2APB are in contact with the hydrophobic side of the amphipathic NTH, in close proximity to the amino
149 acids M1, G5, and L9. The lipid-2 density observed previously in the Cx32-apo structure [39] is located
150 nearby and may contribute to 2APB binding. As we have imposed the D6 symmetry, we have modelled
151 six 2APB molecules occupying the site A. Considering the apparent affinity of 2APB for Cx32 and the
152 drug concentration used for cryo-EM structure determination, modeling of six 2APB molecules is
153 appropriate (keeping in mind the results of the PFC analysis, which suggest some variability in site A
154 occupancy).

155 **Binding of MFQ and 2APB to site M.** The site M is formed by I33, L36, V37, A40, E41, S79, and
156 I82 of one subunit, and M34 and V38 of the neighbouring subunit, and is thus largely hydrophobic (**Fig.
157 3b,c**, Extended Data Fig. 13b,c). However, S79 and E41 may be involved in hydrogen bond formation
158 with the hydroxyl and/or amine group of MFQ, and the amine group of 2APB. Our data clearly
159 implicate this site in functional regulation of Cx32. Consistent with this, mutations of several amino
160 acid residues located within this site (M34, V38, A40, and E41) are involved in the onset of the X-
161 linked Charcot-Marie-Tooth (CMT1X), a Cx32-linked connexinopathy [6], highlighting the functional
162 importance of site M in channel function under physiological and pathophysiological conditions.

163 To biochemically test whether inhibition of Cx32 by MFQ and 2APB is mediated by site M binding we
164 generated single amino acid residue mutants V37T, V37I, V37W, V38W, S78F, E41D, and E41A. The
165 mutants were aimed to disrupt the binding site by either steric hinderance, change of electrostatic
166 properties, and/or disruption of polar bonds between the drug and the binding site. Each of the mutants
167 could be successfully expressed in HEK293F cells (Extended Data Fig. 1c), albeit at different
168 expression levels. Except for V37T, all mutants formed the GJ plaques to approximately an equal extent
169 (Extended Data Fig. 1a-b). HC dye uptake assays showed that all of the mutants have a decreased basal
170 permeability to the dye compared to wild-type Cx32, likely reflecting the suboptimal solute
171 translocation pathway properties in the mutant pores (Extended Data Fig. 2c-k). The effect of the two
172 drugs on the mutants is reduced (with the exception of V37T and V37I and MFQ), suggesting that
173 mutating these amino acid residues disrupts drug binding (Extended Data Fig. 2). V37T and V37I are
174 less bulky and likely do not alter the site M properties sufficiently to prevent drug binding, particularly
175 when other amino acid residues in this site are involved in the drug interaction.

176 To probe the effects of MFQ and 2APB on GJC function, we selected V37I and V37W mutants, based
177 on their distinct sensitivity to the two drugs in HC assays. Consistent with the HC inhibition of the HC
178 result, the gap-FRAP experiments showed that V37W GJCs were not sensitive to MFQ and 2APB
179 treatment, pointing to the disruption of site M as a drug binding site (**Fig. 3d,e**, Extended Data Fig.
180 2a,b). In contrast, drug sensitivity of V37I in GJC permeability assays was similar to that of the wild-
181 type Cx32 (**Fig. 3f,g**, Extended Data Fig. 2a,b). Thus, substitution of V37 in site M with a bulky side
182 chain disrupts MFQ and 2APB sensitivity in cellular assays of Cx32 HC and GJC function, indicating
183 that site M is the primary inhibitory site for small molecule inhibitors. Site A additionally is engaged
184 by 2APB, causing a conformational change and stabilizing the NTH.

Influence of drug binding on Cx32 GJC pore characteristics. MFQ and 2APB have distinct effects on Cx32 channel conformation. Binding of 2APB to site A and the concomitant rearrangement of the NTH reduces the pore radius from ~15 Å to only ~2 Å (**Fig. 4a,b**). Interestingly, binding of 2APB to site M does not result in a decrease of the pore radius: a substantial gap remains between the drugs arranged radially within the pore. Instead of a mere steric obstruction, 2APB binding changes the electrostatic properties of the channel pore making it more hydrophobic (**Fig. 4c,e**, Extended Data Fig. 13d). Likewise, MFQ binding to site M decreases the pore diameter only slightly, concomitant with the changes in the electrostatic potential of the pore (**Fig. 3d**, Extended Data Fig. 13d). Binding of two "rings" of MFQ (or 2APB) to the site M regions of connexons linked within the GJC introduces two hydrophobic barriers in the way of the solutes moving through the channel. Thus, although the pore dimensions appear to be unchanged due to only a minor steric hindrance, free movement of ions or small molecules through the newly formed hydrophobic drug ring inside the pore is restricted. Moreover, binding of the drugs to site M likely neutralizes the residue E41, a polar residue within the connexin pore, playing a key role in voltage gating of the channel [42]. Thus, the combined steric and electrostatic effects of drug-binding to site M likely underlies the small molecule-mediated inhibition of Cx32.

MFQ binds to site M of Cx43 GJC. Our functional and structural data on MFQ and 2APB suggest that site M likely serves as the primary site for inhibitor action in Cx32 GJC. To determine whether site M is a universal inhibitory drug binding pocket in connexins, we analyzed the effects of MFQ on Cx43 using cryo-EM (**Fig. 5a-c**) and functional analysis in cell-based activity assays (**Fig. 5d**).

MFQ has been previously shown to inhibit GJC activity in Cx43-coupled N2A [26] and RIN cells [38]. Using cellular assays in HEK293F cells we observed its inhibitory effect on Cx43 GJC-mediated dye transfer (**Fig. 5d**). Cryo-EM structure determination of the Cx43 GJC in complex with MFQ at 3.7 Å resolution revealed a state of Cx43 similar to that observed previously in Cx43-apo [40,41] (**Fig. 5a**, Extended Data Fig. 14-16). However, similar to Cx32 GJC, a prominent additional density corresponding to MFQ was observed within the region corresponding to site M (**Fig. 5b**). The limited quality of site M density only allowed us to model MFQ using the higher resolution structure of Cx36-MFQ as a template (**Fig. 5a;** PDB ID: 8QOJ). Similar to Cx32, while leaving a substantial opening inside the pore, MFQ binding causes radical changes in the electrostatic properties of the solute translocation pathway, generating two hydrophobic barriers within the channel (**Fig. 5e**).

To functionally validate our structural observations in Cx43 we analyzed GJC sensitivity of the G38W mutant to MFQ (**Fig. 5d,** *inset*). This mutation is equivalent to V37W in Cx32, which is insensitive to MFQ-mediated inhibition of HC and GJC permeability. The G38W mutant retained the basic function as a GJC, but lost sensitivity to MFQ (**Fig. 5d**). In the gap-FRAP assays the ability of MFQ to block the channel function was lost, confirming that site M is the site of inhibitor action not only in Cx32, but also in Cx43.

Discussion

The structures of Cx32 GJC in complex MFQ and 2APB, and Cx43 GJC in complex with MFQ, along with the high-resolution structures of Cx36 bound to the MFQ analogues (companion manuscript) [37] shine a light on the molecular mechanisms of connexin channel inhibition. The two drug binding sites (sites A and M) correspond to the previously described lipid binding sites that may bind either sterols or the acyl chains of phospholipid molecules [26,39–41]. While binding of phospholipids to site A may stabilize the NTH in a closed conformation [40,41], the functional properties of the site M have not been investigated prior to this study [39–41,43]. Our results suggest that drug binding to site A may affect NTH-mediated connexin pore gating (**Fig. 6**). Our functional studies as well as previous work on the effect of 2APB on Cx32 HC and GJC permeation [35,44] show that 2APB inhibits Cx32 channels, whereby we observe that its effect is mediated by the observed NTH rearrangements. Thus, the obtained Cx32 GJC reconstruction in complex with 2APB likely represents a closed conformation of the channel.

In contrast to the site A, small molecule binding to site M does not lead to dramatic changes in the pore radius. The pore dimensions of the MFQ-occupied Cx32 or Cx43 leave a substantial opening within the

236 pore region. However, binding of a drug to the six binding sites per connexon within the GJC
237 dramatically affects the electrostatic potential of the pore, introducing two hydrophobic barriers into
238 the solute translocation pathway. A link between pore electrostatics and permeability has been observed
239 in Cx31.3 HC, where introduction of R15G point mutation altered the surface charge at the cytoplasmic
240 pore opening from positive to neutral, without any associated pore radius changes, resulting in increased
241 permeability to ATP [45]. The site M of Cx32 is positioned close to the residue E41 (Extended Data Fig.
242 17, E42 in Cx43, E43 in Cx36), a highly conserved residue among connexins implicated in voltage
243 gating [42,46,47]. The equivalent glutamate residues in Cx26 and Cx46 have been proposed to be a part of
244 the channel's slow gate; the E42Q mutations in Cx26 and Cx46 shown to abrogated the HC currents
245 [42,47]. It is likely that the changes in electrostatic potential adjacent to the site M / E41 region will
246 dramatically affect channel permeability.

247 Although both MFQ and 2APB are relatively weak inhibitors for Cx32 and Cx43, our *in vitro* results
248 are close to the previously reported IC_{50} values (25 μM for MFQ Cx32 GJC coupling inhibition in RIN
249 cells [38] and 47 μM for 2APB inhibition of Cx32 HCs [35]). Nevertheless, the identification of the binding
250 sites of these inhibitors in Cx32 and Cx43 GJCs delivers the first insights crucial for the future
251 development of potent and highly specific chemical agents that act on connexin channels. The connexin
252 inhibitors may be particularly favorable in treatment of connexin HC-related diseases and related
253 pathologies (such as healing of wounds [19], arrhythmia [48], inflammation [49]), which may be normally
254 caused by increased HC function [10,16]. Moreover, specific drug capable of uncoupling the GJC-
255 connected cells may be highly desirable particularly in non-metastasized primary tumors [50–52]. Our
256 structures provide a path to a strategy for targeting the connexin channels using structure-based drug
257 design approaches. The site A, which maps to a highly dynamic gating region of the connexin channels,
258 may offer advantages as a binding site more accessible from the cytosol, with the caveat of relatively
259 poor definition of this site in the known connexin channels due to high degree of observed mobility in
260 the NTH. In contrast, the site M is located in a rigid and structurally conserved pocket in each of the
261 connexin channels. The site has very favorable features for designing specific compounds with high
262 selectivity for a connexin of interest. The novel mode of drug binding and inhibition via site M observed
263 in Cx32, Cx43 and Cx36 may offer additional advantages in designing new compounds with unique
264 properties, such as cooperative binding or selective channel permeability.

265

266 **References**

267

268 1. Dbouk, H. A., Mroue, R. M., El-Sabban, M. E. & Talhouk, R. S. Connexins: a myriad of functions
269 extending beyond assembly of gap junction channels. *Cell Commun. Signal.* **7**, 4 (2009).
270 2. Nielsen, M. S. *et al.* Gap Junctions. *Compr. Physiol.* **2**, 10.1002/cphy.c110051 (2012).
271 3. Totland, M. Z., Rasmussen, N. L., Knudsen, L. M. & Leithe, E. Regulation of gap junction intercellular
272 communication by connexin ubiquitination: physiological and pathophysiological implications. *Cell. Mol.*
273 *Life Sci.* **77**, 573–591 (2020).
274 4. Kurtenbach, S., Kurtenbach, S. & Zoidl, G. Gap junction modulation and its implications for heart function.
275 *Front. Physiol.* **5**, (2014).
276 5. Naus, C. C. G. & Bani-Yaghoub, M. Gap Junctional Communication in the Developing Central Nervous
277 System. *Cell Biol. Int.* **22**, 751–763 (1998).
278 6. Bortolozzi, M. What's the Function of Connexin 32 in the Peripheral Nervous System? *Front. Mol.*
279 *Neurosci.* **11**, (2018).
280 7. El-Sabban, M. E. *et al.* ECM-induced gap junctional communication enhances mammary epithelial cell
281 differentiation. *J. Cell Sci.* **116**, 3531–3541 (2003).
282 8. Glass, A. M., Snyder, E. G. & Taffet, S. M. Connexins and pannexins in the immune system and lymphatic
283 organs. *Cell. Mol. Life Sci.* **72**, 2899–2910 (2015).
284 9. Yamasaki, H. *et al.* Role of connexin (gap junction) genes in cell growth control and carcinogenesis. *C. R.*
285 *Acad. Sci. III* **322**, 151–159 (1999).
286 10. Delmar, M. *et al.* Connexins and Disease. *Cold Spring Harb. Perspect. Biol.* **10**, a029348 (2018).
287 11. Paznekas, W. A. *et al.* Connexin 43 (GJA1) mutations cause the pleiotropic phenotype of oculodentodigital
288 dysplasia. *Am. J. Hum. Genet.* **72**, 408–418 (2003).
289 12. Shuja, Z., Li, L., Gupta, S., Meşe, G. & White, T. W. Connexin26 mutations causing palmoplantar
290 keratoderma and deafness interact with connexin43, modifying gap junction and hemichannel properties. *J.*
291 *Invest. Dermatol.* **136**, 225–235 (2016).
292 13. Lee, J. R. & White, T. W. Connexin-26 mutations in deafness and skin disease. *Expert Rev. Mol. Med.* **11**,
293 e35 (2009).
294 14. Yamasaki, H., Mesnil, M., Omori, Y., Mironov, N. & Krutovskikh, V. Intercellular communication and
295 carcinogenesis. *Mutat. Res.* **333**, 181–188 (1995).

296 15. Srinivas, M., Verselis, V. K. & White, T. W. Human diseases associated with connexin mutations.
297 *Biochim. Biophys. Acta BBA - Biomembr.* **1860**, 192–201 (2018).
298 16. Laird, D. W. & Lampe, P. D. Therapeutic strategies targeting connexins. *Nat. Rev. Drug Discov.* **17**, 905–
299 921 (2018).
300 17. Sellitto, C., Li, L. & White, T. W. Connexin hemichannel inhibition ameliorates epidermal pathology in a
301 mouse model of keratitis ichthyosis deafness syndrome. *Sci. Rep.* **11**, 24118 (2021).
302 18. De Vuyst, E. *et al.* Pharmacological modulation of connexin-formed channels in cardiac pathophysiology.
303 *Br. J. Pharmacol.* **163**, 469–483 (2011).
304 19. Montgomery, J., Ghatnekar, G. S., Grek, C. L., Moyer, K. E. & Gourdie, R. G. Connexin 43-Based
305 Therapeutics for Dermal Wound Healing. *Int. J. Mol. Sci.* **19**, 1778 (2018).
306 20. Davidson, J. S. & Baumgarten, I. M. Glycyrrhetinic acid derivatives: a novel class of inhibitors of gap-
307 junctional intercellular communication. Structure-activity relationships. *J. Pharmacol. Exp. Ther.* **246**,
308 1104–1107 (1988).
309 21. Délèze, J. & Hervé, J. C. Effect of several uncouplers of cell-to-cell communication on gap junction
310 morphology in mammalian heart. *J. Membr. Biol.* **74**, 203–215 (1983).
311 22. Eskandari, S., Zampighi, G. A., Leung, D. W., Wright, E. M. & Loo, D. D. F. Inhibition of gap junction
312 hemichannels by chloride channel blockers. *J. Membr. Biol.* **185**, 93–102 (2002).
313 23. Puebla, C., Retamal, M. A., Acuña, R. & Sáez, J. C. Regulation of Connexin-Based Channels by Fatty
314 Acids. *Front. Physiol.* **8**, (2017).
315 24. Rubinos, C., Sánchez, H. A., Verselis, V. K. & Srinivas, M. Mechanism of inhibition of connexin channels
316 by the quinine derivative N-benzylquininium. *J. Gen. Physiol.* **139**, 69–82 (2012).
317 25. David C. Spray, Mathhew G. Hopperstad, M. S. Quinine blocks specific gap junction channel subtypes.
318 *PNAS* **98**, 10942–10947 (2001).
319 26. Miduturu Srinivas, S. J. C. Potent block of Cx36 and Cx50 gap junction channels by mefloquine. *PNAS*
320 **101**, 12364–12369 (2004).
321 27. Natha, C. M., Vemulapalli, V., Fiori, M. C., Chang, C.-W. T. & Altenberg, G. A. Connexin hemichannel
322 inhibitors with a focus on aminoglycosides. *Biochim. Biophys. Acta BBA - Mol. Basis Dis.* **1867**, 166115
323 (2021).
324 28. Ghosh, D. K., Kumar, A. & Ranjan, A. Cellular targets of mefloquine. *Toxicology* **464**, 152995 (2021).

325 29. Nevin, R. L. Epileptogenic potential of mefloquine chemoprophylaxis: a pathogenic hypothesis. *Malar. J.*
326 **8**, 188 (2009).
327 30. Nevin, R. L. & Byrd, A. M. Neuropsychiatric Adverse Reactions to Mefloquine: a Systematic Comparison
328 of Prescribing and Patient Safety Guidance in the US, UK, Ireland, Australia, New Zealand, and Canada.
329 *Neurol. Ther.* **5**, 69–83 (2016).
330 31. Croft, A. M. & Herxheimer, A. Adverse effects of the antimalaria drug, mefloquine: due to primary liver
331 damage with secondary thyroid involvement? *BMC Public Health* **2**, 6 (2002).
332 32. Jeanson, T. *et al.* Potentiation of Amitriptyline Anti-Hyperalgesic-Like Action By Astroglial Connexin 43
333 Inhibition in Neuropathic Rats. *Sci. Rep.* **6**, 38766 (2016).
334 33. Morihara, H. *et al.* 2-aminoethoxydiphenyl borate provides an anti-oxidative effect and mediates
335 cardioprotection during ischemia reperfusion in mice. *PLOS ONE* **12**, e0189948 (2017).
336 34. Lin, L., Dai, F., Chen, Z. & Cai, L. In Vitro Treatment with 2-APB Inhibits the Inflammation in Nasal
337 Polyps. *Otolaryngol.--Head Neck Surg. Off. J. Am. Acad. Otolaryngol.-Head Neck Surg.* **153**, 461–467
338 (2015).
339 35. Tao, L. & Harris, A. L. 2-Aminoethoxydiphenyl Borate Directly Inhibits Channels Composed of
340 Connexin26 and/or Connexin32. *Mol. Pharmacol.* **71**, 570–579 (2007).
341 36. David C. Spray, D. B. Block of Specific Gap Junction Channel Subtypes by 2-Aminoethoxydiphenyl
342 Borate (2-APB). *J. Pharmacol. Exp. Ther.* **319**, 1452–1458.
343 37. Ding, X. *et al.* Structural basis of connexin-36 gap junction channel inhibition. 2023.12.09.570920 Preprint
344 at https://doi.org/10.1101/2023.12.09.570920 (2023).
345 38. Picoli, C. *et al.* Human Connexin Channel Specificity of Classical and New Gap Junction Inhibitors. *J.*
346 *Biomol. Screen.* **17**, 1339–1347 (2012).
347 39. Qi, C. *et al.* Structures of wild-type and selected CMT1X mutant connexin 32 gap junction channels and
348 hemichannels. *Sci. Adv.* **9**, eadh4890.
349 40. Jae-Sung Woo, H.-J. L. Conformational changes in the human Cx43/GJA1 gap junction channel visualized
350 using cryo-EM. *Nat. Commun.* **19**, (2023).
351 41. Chao, Q. *et al.* Structure of the connexin-43 gap junction channel in a putative closed state. *eLife* **12**,
352 (2023).
353 42. Pinto, B. I. *et al.* Charged Residues at the First Transmembrane Region Contribute to the Voltage
354 Dependence of the Slow Gate of Connexins. *J. Biol. Chem.* **291**, 15740–15752 (2016).

355 43. Lee, S.-N. *et al.* Cryo-EM structures of human Cx36/GJD2 neuronal gap junction channel. *Nat. Commun.*
356 **14**, 1347 (2023).
357 44. Comollo, T. W. Molecular Modeling Suggests Homologous 2-APB Binding Sites in Connexins 26 and 32.
358 287326 Preprint at https://doi.org/10.1101/287326 (2018).
359 45. Lee, H.-J. *et al.* Cryo-EM structure of human Cx31.3/GJC3 connexin hemichannel. *Sci. Adv.* **6**, eaba4996
360 (2020).
361 46. Maeda, S. *et al.* Structure of the connexin 26 gap junction channel at 3.5 Å resolution. *Nature* **458**, 597–
362 602 (2009).
363 47. Harris, A. L. Emerging issues of connexin channels: biophysics fills the gap. *Q. Rev. Biophys.* **34**, 325–472
364 (2001).
365 48. Leybaert, L. *et al.* Connexin hemichannels as candidate targets for cardioprotective and anti-arrhythmic
366 treatments. *J. Clin. Invest.* **133**, (2023).
367 49. Cliff, C. L. *et al.* Connexin 43: A Target for the Treatment of Inflammation in Secondary Complications of
368 the Kidney and Eye in Diabetes. *Int. J. Mol. Sci.* **23**, 600 (2022).
369 50. Aasen, T., Mesnil, M., Naus, C. C., Lampe, P. D. & Laird, D. W. 'Gap Junctions and Cancer:
370 Communicating for 50 Years'. *Nat. Rev. Cancer* **16**, 775–788 (2016).
371 51. Zibara, K. *et al.* Anti-angiogenesis therapy and gap junction inhibition reduce MDA-MB-231 breast cancer
372 cell invasion and metastasis in vitro and in vivo. *Sci. Rep.* **5**, 12598 (2015).
373 52. Chen, Q. *et al.* Carcinoma-astrocyte gap junctions promote brain metastasis by cGAMP transfer. *Nature*
374 **533**, 493–498 (2016).
375
376

Acknowledgments: We would like to thank M. Peterek (ScopeM, ETH Zurich) and E. Poghosyan (EM Facility, Paul Scherrer Institute) for expert support in cryo-EM data collection, and P. Afanasyev (Cryo-EM Knowledge Hub, ETH Zurich) for data processing advice. We thank S. Bliven and M. Caubet-Serrabou for support in high-performance computing. We thank E. Lazzarin (Medical University of Vienna) for advice on performing APBS calculations.

Funding: The work was supported by the Swiss National Science Foundation (grant 184915 to V.M.K).

Author contributions:

Conceptualization: VMK

Methodology: PL, YH, XD, CQ, AV, VMK

Investigation: PL, YH, XD, CQ, AV, VMK

Visualization: PL, YH, VMK

Funding acquisition: VMK

Project administration: VMK

Supervision: VMK

Writing – original draft: PL, YH, VMK

Writing – review & editing: PL, YH, XD, CQ, AV, VMK

Competing interests: The authors declare no competing interests.

Data and materials availability: The cryo-EM density maps and model coordinates have been deposited to the Electron Microscopy Data Bank and Protein Data Bank with the following accession numbers: PDB ID 8QJF, EMD-18446; PDB ID 8QK6, EMD-18457; PDB-ID 8QJH, EMD-ID 18447; PDB-ID 8QKI, EMD-18463; PDB-ID 8QKO, EMD-18468. All data required to evaluate the conclusions in this paper are present in the paper and in the Supplementary Materials.

Supplementary Materials

Materials and Methods

Extended Data Figs. 1 to 17

Extended Data Table 1

References (1-22)

Figures

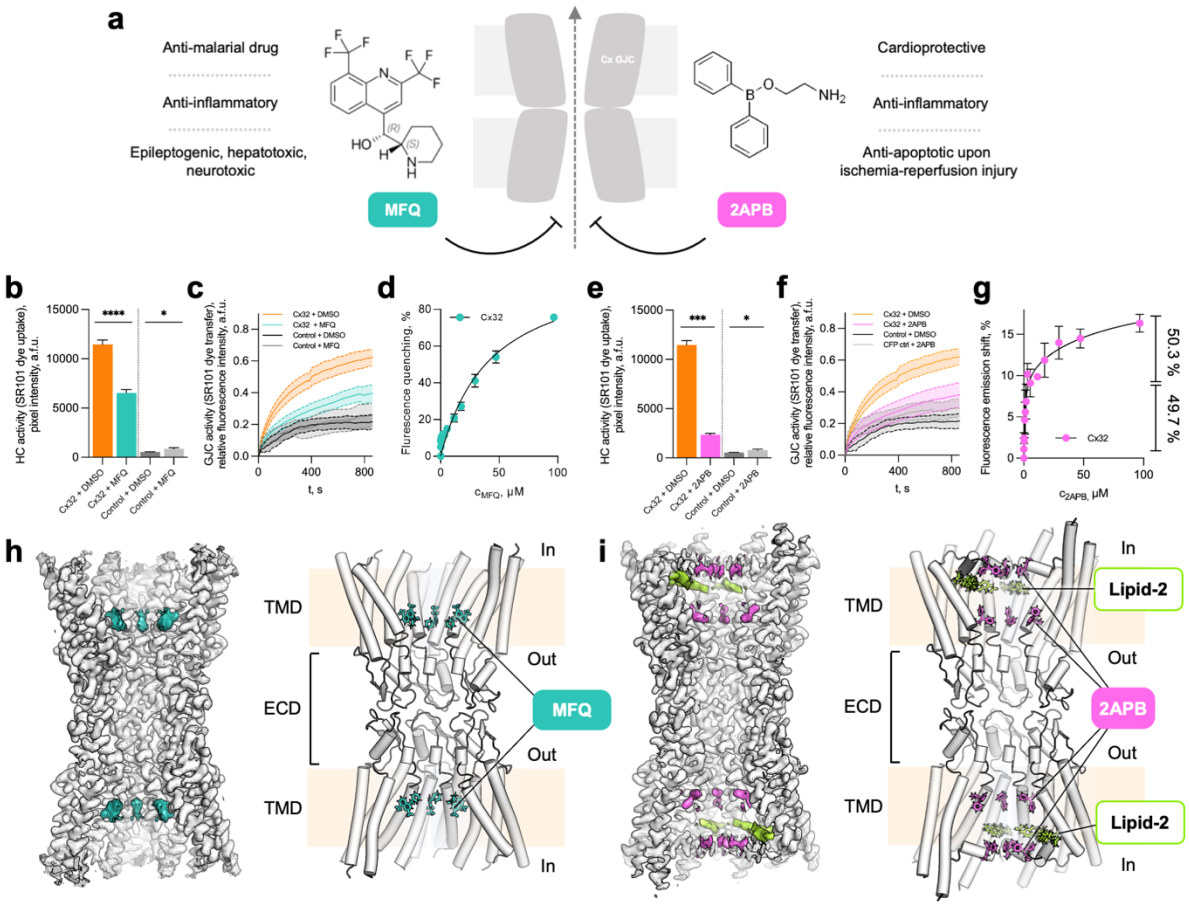

Fig. 1. Analysis of Cx32 channel inhibition by MFQ and 2APB. a, Schematic representation of connexin inhibition by MFQ and 2APB. **b,** Dye uptake of Cx32 HC and mock-transfected control cells upon treatment with MFQ or DMSO (drug solvent) (Cx32: MFQ, n = 1183; DMSO, n = 1109; Control: MFQ, n = 1047; DMSO, n = 1016). The HC dye-uptake values were compared using Games-Howell's multiple comparisons test: **** - P < 0.0001, *** - P < 0.001, ** - P < 0.01, * - P < 0.05, ns – P > 0.05. *n – number of measured cells; all experiments were performed in experimental triplicates.* **c,** GJC permeability in Cx32 and mock-transfected control cells upon MFQ, or DMSO treatment (Cx32: DMSO, n = 12; MFQ, n = 16; Control: DMSO, n = 7; MFQ, n = 13). **d,** Cx32 tryptophan fluorescence quenching upon MFQ treatment (n = 3). **e,** Dye uptake of Cx32 HC and mock-transfected control cells upon treatment with 2APB or DMSO (Cx32: 2APB, n = 911; DMSO, n = 1109; Control: 2APB, n = 1047; DMSO, n = 1016). *n – number of measured cells; all experiments were performed in experimental triplicates.* **f,** GJC permeability for Cx32 and mock-transfected control upon 2APB, or DMSO treatment (Cx32: DMSO, n = 12; 2APB, n = 15; Control: DMSO, n = 7; 2APB, n = 12). **g,** Spectral shift of tryptophan fluorescence upon 2APB titration (n = 3). The values (%) on the right side in **d** and **g** indicate the distribution of the calculated low and high affinity binding sites. All data is represented as mean ± SEM. **h,** Side views of cryo-EM map and model of Cx32 GJC in complex with MFQ. **i,** Same as h, for Cx32-2APB (level = 4σ). Additional densities in h and i, interpreted to be MFQ and 2APB respectively, are illustrated with colored features. TMD – transmembrane domain; ECD – extracellular domain; In – intracellular side; Out – extracellular side.

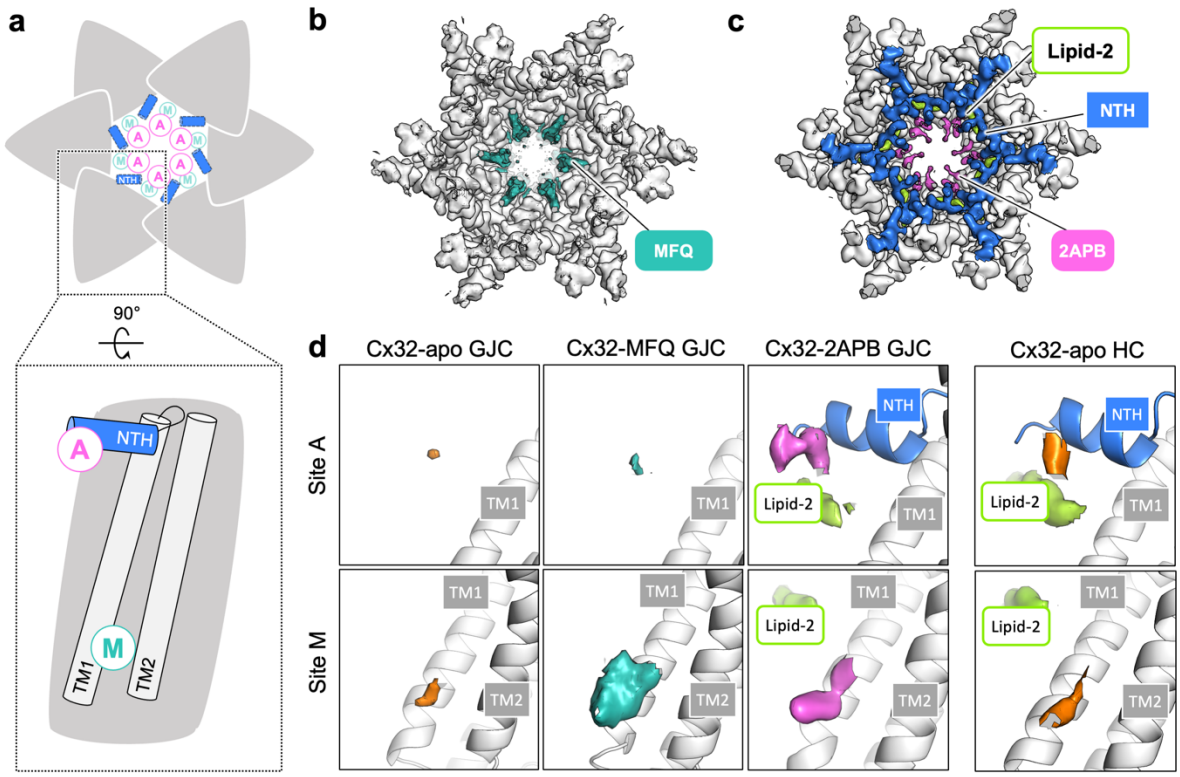

Fig. 2. Locations of the MFQ and 2APB binding sites in the Cx32 GJC. a, Schematic representation of putative MFQ and 2APB binding sites A and M in the Cx32 GJC. **b-c,** Views of the Cx32-MFQ (b) and Cx32-2APB maps, contoured at 4σ. **d-e,** A comparison of the densities at sites A and M in Cx32-apo GJC and Cx32-MFQ GJC, Cx32-2APB GJC (d) and Cx32-apo HC (e) (all maps contoured at 3σ). TM – transmembrane helix, NTH – N-terminal helix.

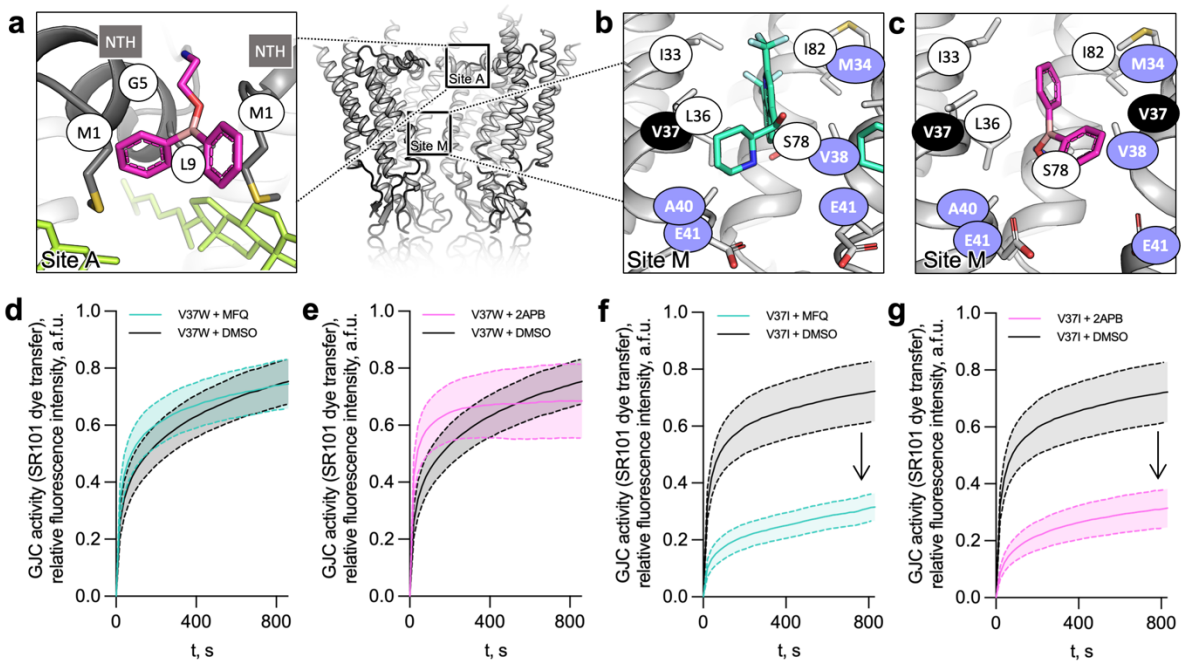

Fig. 3. Molecular details of the inhibitor binding sites in Cx32. **a,** Locations of site A and M are shown with the boxes (*right*). Left: site A. Residues (side chains shown as sticks) constituting the site A, within 4 Å of the bound 2APB molecule, are shown with white labels. The sterol molecule (green) is located in close vicinity of the site A. **b-c,** Site M. Side chains of the residues in close proximity of the MFQ (b) or 2APB (c) are shown as sticks. Purple labels indicate residues linked to CMT1X disease. **d-g,** GJC permeability of V37W and V37I Cx32 mutants upon treatment with MFQ (d, f) and 2APB (e, g). The GJC activity values are shown as mean ± SEM; for d, n = 20 (DMSO) and n = 18 (MFQ); for e, n = 20 (DMSO) and n = 16 (2APB); for f, n = 17 (DMSO) and n = 19 (MFQ); for g, n = 17 (DMSO) and n = 20 (2APB).

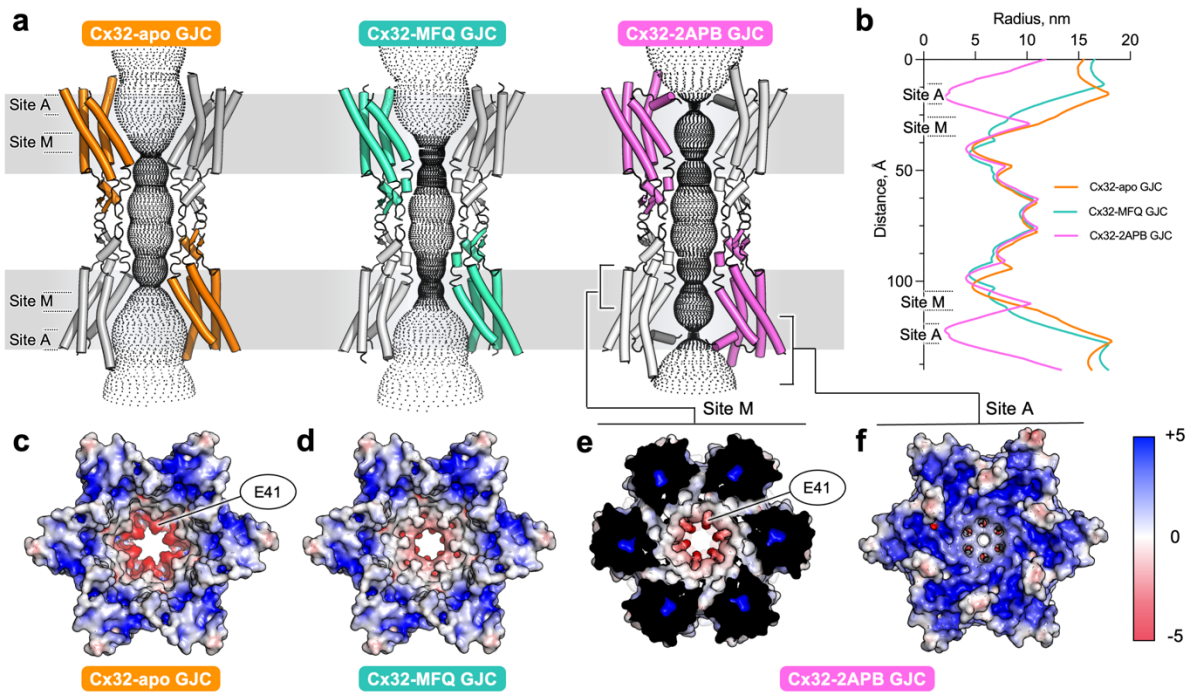

Fig. 4. Effect of drug binding to site A and M on Cx32 GJC pore properties. a, Diffusive pathways for the solutes of Cx32 and Cx32 in complex with MFQ or 2APB, calculated using HOLE. **b,** Pore radii along the pore, calculated using HOLE (shown in a). **c-d,** Electrostatic surface potential representations of Cx32-apo GJC (c), Cx32-MFQ (d). **e,** The clipped view of Cx32-2APB revealing the site M. **f,** The unclipped view of Cx32-2APB (as in c and d).

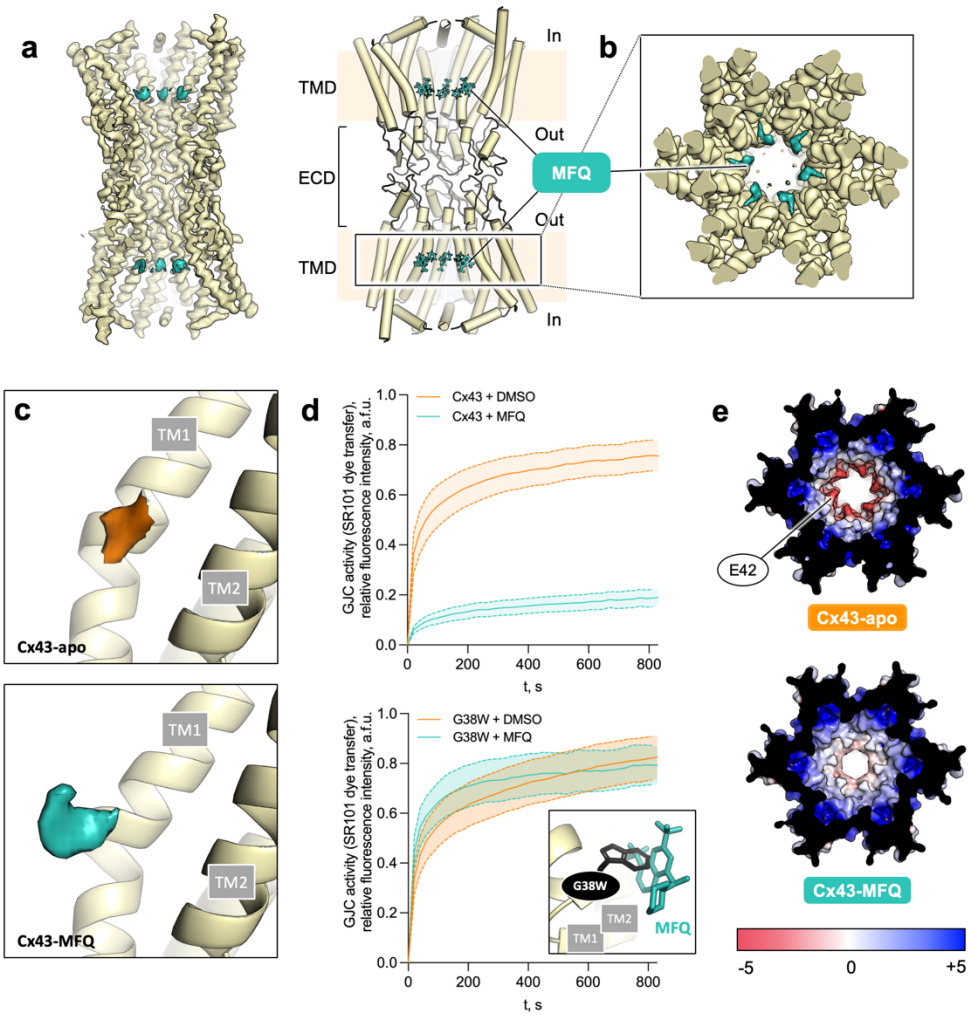

Fig. 5. Functional and structural analysis of MFQ effect on Cx43 GJC. a, A view of the cryo-EM map and model of Cx43 GJC in complex with MFQ. **b,** Cryo-EM map of Cx43-MFQ, viewed from the cytosolic side; a clipped view, excluding the NTH density is shown. **c,** Comparison of site M density of Cx43-apo GJC and Cx43-MFQ GJC (contoured at 3.3σ). **d,** GJC permeability of WT Cx43 (f) and G38W (g) with or without MFQ treatment (n = 15). All data in e-g are represented as mean ± SEM. *Inset:* A G38W mutation sterically hinders MFQ binding, with the side chain of W38 clashing with the ligand. **e,** Comparison of electrostatic surface potential of Cx43-apo (PDB ID: 7Z1T) and Cx43-MFQ GJCs.

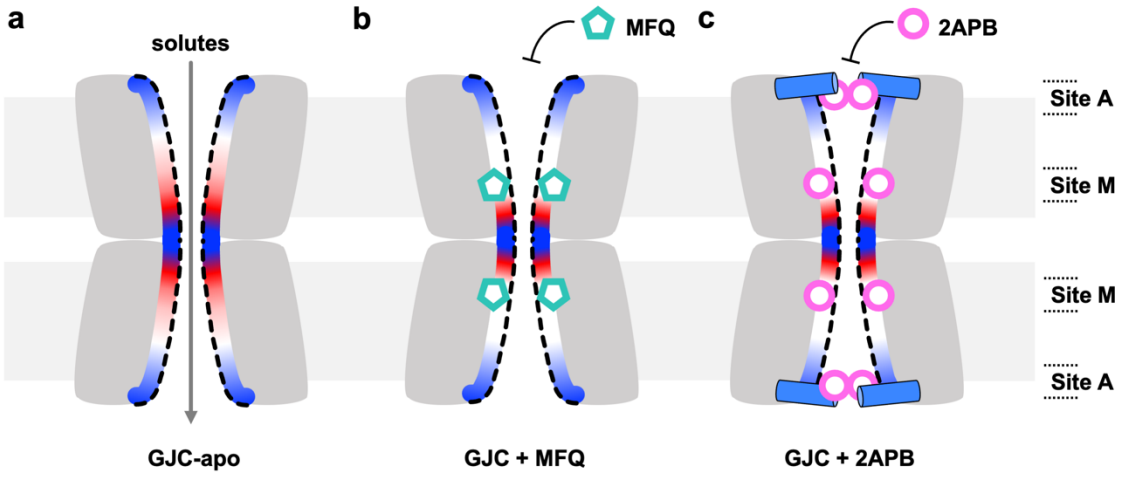

Fig. 6. Mechanism of connexin channel inhibition via sites A and M. a, In the absence of the inhibitors, the connexin GJCs allow free passage of solutes (<1.5 kDa). **b,** Binding of MFQ to site M introduces and electrostatic barrier in the pore, reducing GJCs permeability. **c,** 2APB binds to site M and to site A, causing NTH rearrangement and constriction of the pore entrance.